Thermochemistry and Kinetics of Silicon Hydride Cluster Formation during Thermal Decomposition of Silane

Mark T. Swihart*,† and Steven L. Girshick

Department of Mechanical Engineering, University of Minnesota, 111 Church Street SE, Minneapolis, Minnesota 55455

Received: August 12, 1998; In Final Form: November 3, 1998

Product contamination by particles nucleated within the processing environment often limits the deposition rate during chemical vapor deposition processes. A fundamental understanding of how these particles nucleate could allow higher growth rates while minimizing particle contamination. Here we present an extensive chemical kinetic mechanism for silicon hydride cluster formation during silane pyrolysis. This mechanism includes detailed chemical information about the relative stability and reactivity of different possible silicon hydride clusters. It provides a means of calculating a particle nucleation rate that can be used as the nucleation source term in aerosol dynamics models that predict particle formation, growth, and transport. A group additivity method was developed to estimate thermochemical properties of the silicon hydride clusters. Reactivity rules for the silicon hydride clusters were proposed based on the group additivity estimates for the reaction thermochemistry and the analogous reactions of smaller silicon hydrides. These rules were used to generate a reaction mechanism consisting of reversible reactions among silicon hydrides containing up to 10 silicon atoms and irreversible formation of silicon hydrides containing 11−20 silicon atoms. The resulting mechanism was used in kinetic simulations of clustering during silane pyrolysis in the absence of any surface reactions. Results of those simulations are presented, along with reaction path analyses in which key reaction paths and rate-limiting steps are identified and discussed.

I. Introduction

Chemical vapor deposition (CVD) of silicon from silane is an important and widely used process in the microelectronics industry. In many cases deposition rates, and therefore throughput and equipment utilization, are limited by the homogeneous gas-phase nucleation of particles that contaminate the product. An understanding of particle nucleation, growth, and transport in these reactors would allow selection of reactor designs and operating conditions that optimize growth rate and product properties while reducing or eliminating particle formation. A fundamental understanding of these processes could also aid in the development of methods for producing silicon nanoparticles or nanostructured materials via vapor-phase nucleation and growth of particles.

Thermal CVD of silicon from silane has been widely studied both experimentally and theoretically. In particular, Breiland, Coltrin, Ho, and co-workers at Sandia National Laboratories have made extensive comparisons of mathematical models and experimental measurements of silicon growth rates and reactive species concentration profiles.[1−7] There is also a substantial body of work on the kinetics of gas-phase reactions of small silicon hydrides.[8−26] On the basis of this body of research, models of thermal CVD of silicon from silane can now predict film growth rates and precursor utilization with reasonable accuracy and reliability, at least under conditions where particle formation is negligible. However, understanding of the processes that lead to gas-phase particle nucleation is still quite limited, and models for nucleation and growth of particles in this system do not have the level of predictive capability that has been achieved in modeling film growth rates and gas-phase chemical composition.

Detailed kinetic modeling of silane pyrolysis, including reactions that lead to formation of silicon hydride clusters that grow into particles, can give insights into particle nucleation mechanisms and the factors that control the onset of particle formation. The kinetic model provides a rate of formation of silicon hydride clusters of a given size. This cluster production rate can be taken as the nucleation rate for use in aerosol dynamics models that allow prediction of particle concentration, size, and spatial distribution. Yuuki et al.[27] presented a simple particle formation mechanism that included species with up to five silicon atoms and formation of particles from Si_5H_{12}. Giunta et al.[28] developed a larger mechanism that included linear silanes (saturated Si_nH_{2n+2}), silylenes (divalent Si_nH_{2n}), and silenes (Si_nH_{2n} with a formal double bond) containing up to 10 silicon atoms. The higher silanes were formed by insertions of silylenes into silanes, i.e.

$$\text{silylene}_n + \text{silane}_m \rightarrow \text{silane}_{n+m} \qquad (1)$$

where n and m denote the number of silicon atoms in the molecule. The silylenes were formed by elimination of molecular hydrogen from the corresponding silane and by elimination from the larger silanes (the reverse of reaction 1). Frenklach et al.[29] presented a similar and somewhat larger mechanism for particle formation by silicon hydride clustering. In addition to polymerization by silylene insertions as represented in reaction 1, they considered clustering reactions of atomic silicon and some interactions of the pure silicon clusters with hydrogen. In both of these studies, the kinetics for reactions of higher silanes

† Current address: Department of Chemical Engineering, SUNY Buffalo, Buffalo, New York 14260-4200. E-mail: swihart@eng.buffalo.edu.

10.1021/jp983358e CCC: $18.00 © 1999 American Chemical Society
Published on Web 12/16/1998

and silylenes (n or $m > 2$) were assumed to be identical to those for the analogous reaction of disilane. For example, the forward rate coefficient of $SiH_2 + Si_nH_{2n+2} \rightarrow Si_{n+1}H_{2n+4}$, $n \geq 3$ was assumed to be equal to that of $SiH_2 + Si_2H_6 \rightarrow Si_3H_8$. In addition to these models of clustering via polysilane formation, models for homogeneous nucleation of pure silicon from its supersaturated vapor have been presented in the literature. Several groups used variations of classical nucleation theory[30−33] to calculate the nucleation rate. Kelkar et al.[34] took an atomistic approach that utilized the thermodynamic properties of small silicon clusters rather than making the capillarity assumption of classical nucleation theory.

The studies cited above did not consider the formation of cyclic or polycyclic silicon hydride molecules. Veprek and co-workers,[35] in a study of particle formation via reactions of neutral species in a low-pressure silane plasma, hypothesized that formation of rings and more complex three-dimensional structures would play an important role in particle nucleation. They presented an outline of a mechanism for cluster formation and experimental measurements of SiH_2 concentrations and light scattering from particles that supported the general features of their mechanism. However, they did not develop a detailed mechanism or model for the cluster formation or investigate which species or reaction pathways were most important for particle nucleation. In a cluster growth mechanism involving silylenes, we expect ring formation to play an important role, since a silylene with a sufficiently long linear segment can react with itself to form a ring by the same silylene insertion mechanism that leads to cluster growth, i.e.

$$\text{acyclic silylene}_n \rightarrow \text{cyclic silane}_n \qquad (2)$$

This reaction is expected to be exothermic by an amount comparable to other insertions of a silylene into a silane (roughly 50 kcal/mol) if the ring is large enough that ring strain energy is not important. For small rings, it will be less exothermic due to the strain energy of the ring, but the cyclic silane is expected to be more stable than the acyclic silylene even for three-membered rings. Once a ring is formed, it is relatively difficult for it to decompose by silylene elimination (the reverse of reaction 1) since two Si−Si bonds have to be broken to eliminate a silicon-containing molecule from the ring. The same processes lead to the formation of multiple rings, which one can easily imagine evolving into the diamond cubic structure of bulk silicon, which may be viewed as being made up of six-membered rings.

There have been a number of experimental studies of particle formation during thermal decomposition of silane, and some key observations will be summarized here. Slootman and Parent[36] observed a very sharp onset of nucleation with increasing temperature, in one case seeing measured particle concentrations increase by a factor of 10^4 due to a temperature increase of only 2 K. They also observed that the critical temperature for the onset of nucleation was substantially higher in a hydrogen carrier gas than in inert carrier gases. They summarize their own data and results of earlier studies for the critical temperatures and concentrations at which particle formation was observed. Nijhawan et al.[37,38] have made measurements of particle formation in two different low-pressure thermal CVD reactors. Onischuk and co-workers[39−41] have analyzed the hydrogen content and bonding of particles formed during thermal decomposition of silane, as well as the overall kinetics and dependence on reaction conditions. They found that the hydrogen-to-silicon ratio in the solid product ranged from 0.1 to 0.5 and decreased with increasing temperature and increasing reaction time. This indicates that under all of the conditions which they investigated, the final particles are substantially dehydrogenated relative to acyclic polysilanes (that have a hydrogen-to-silicon ratio of about 2) but that the particles are not completely dehydrogenated.

In this work we extend the detailed kinetic modeling of silicon hydride clustering reactions to include (1) thermodynamic properties of silicon hydride clusters with up to 10 silicon atoms calculated using ab initio and group additivity methods, (2) rate parameters estimated based on linear free energy relationships and the reaction thermochemistry, and (3) formation of rings and polycyclic silicon hydride clusters. This allows us to identify key species and reaction pathways leading to particle formation and to investigate the dependence of these pathways on reactor conditions. It also provides us with a means of predicting particle nucleation rates that could be coupled to aerosol dynamics models that would predict particle sizes and concentrations. Section II of this paper outlines the methodology used for calculating the thermochemical properties of silicon hydride clusters and gives key results of those calculations. Section III presents the reaction mechanism developed to describe clustering and the methods used to construct it and to estimate rate parameters. In section IV we show results of kinetic simulations and identify key species and reaction paths that lead to cluster formation over a range of conditions.

II. Thermochemistry of the Silicon Hydrides

Experimental thermochemical data are available only for the smallest silicon hydrides (SiH_4, SiH_2, Si_2H_6). The thermochemistry used in this work is based primarily on the extensive ab initio calculations of Katzer et al.[42] They calculated standard-state enthalpies and entropies for 143 silicon hydride compounds containing up to five silicon atoms using an empirically corrected ab initio methodology. In addition to their published results, they provided us with access to the calculated vibrational frequencies for all of the compounds and additional unpublished data tables.[43] On the basis of their results, we developed a group additivity method that allows estimation of the enthalpy, entropy, and heat capacity of arbitrary silanes, silenes, and silylenes. The group additivity scheme uses the same general methodology that has been used successfully for prediction of the thermochemistry of hydrocarbons.[44] Twenty-six groups were defined, and group contribution values for heat of formation, standard enthalpy, and heat capacity were determined by a linear least-squares fit to the properties of 71 silanes, silylenes, and silenes studied by Katzer et al. The groups used and the corresponding group contribution values are given in Table 1. This set of parameters reproduced the enthalpy of formation, standard entropy, and heat capacity of the 71 compounds with average absolute errors of 0.73 kcal/mol, 0.61 cal/(mol K), and 0.05 cal/(mol K), respectively. The corresponding maximum fitting errors were 3.6 kcal/mol, 1.9 cal/(mol K), and 0.53 cal/(mol K).

In determining the group additivity parameters, the thermodynamic properties of cyclopentasilane (Si_5H_{10}) were altered slightly from the values reported by Katzer et al.[42] This molecule has one very low frequency vibrational mode which is best treated as a pseudorotation, as is done for cyclopentane (C_5H_{10}).[45,46] This treatment lowers the heat of formation and heat capacity by $RT/2$ and $R/2$, respectively, where R is the universal gas constant and T is the absolute temperature. More importantly, it lowers the standard entropy at 298K by 3.3 cal/(mol K). This change is significant because the thermochemistry of cyclopentasilane determines the group values for the five-

TABLE 1: Group Additivity Parameters for Silicon Hydrides[a]

	ΔH_f°	S°	C_p						
group[a]	298	298	300	400	500	600	800	1000	1500
$Si-(H)_3(Si)$	10.14	33.65	9.68	11.57	13.10	14.38	16.36	17.76	19.68
$Si-(H)_2(Si)_2$	9.54	15.74	9.06	10.66	11.83	12.75	14.13	15.08	16.40
$Si-(H)(Si)_3$	7.45	−2.43	8.42	9.64	10.43	11.00	11.80	12.33	13.07
$Si-(Si)_4$	4.40	−22.47	7.94	8.67	9.05	9.25	9.47	9.59	9.75
$Si-(H)_3(Si_a)$	10.03	34.06	9.80	11.67	13.15	14.39	16.34	17.72	19.65
$Si-(H)_2(Si_a)(Si)$	10.15	15.91	9.21	10.78	11.91	12.80	14.14	15.08	16.39
$Si-(H)(Si_a)(Si)_2$	8.99	−2.23	8.75	9.89	10.62	11.14	11.89	12.40	13.10
$Si-(Si_a)(Si)_3$	7.90	−21.58	8.37	8.99	9.29	9.45	9.62	9.70	9.81
$Si-(H)_3(Si_b)$	10.09	16.33	8.48	10.07	11.30	12.28	13.77	14.81	16.24
$Si-(H)_2(Si_b)(Si)$	10.09	−2.52	7.88	9.16	10.00	10.62	11.49	12.08	12.92
$Si-(H)(Si_b)(Si)_2$	5.27	−21.03	7.02	7.97	8.47	8.75	9.06	9.25	9.55
$Si-(Si_b)(Si)_3$	1.22	−39.03	6.32	6.81	6.91	6.84	6.59	6.39	6.15
$Si_a-(H)_2$	33.48	31.87	8.36	9.59	10.50	11.25	12.43	13.29	14.50
$Si_a-(H)(Si)$	31.08	13.81	7.30	8.25	8.89	9.37	10.07	10.55	11.20
$Si_a-(Si)_2$	26.77	−3.63	6.08	6.71	7.09	7.33	7.60	7.73	7.85
Si_b	66.08	50.31	8.07	8.86	9.53	10.13	11.14	11.86	12.84
C_3	36.13	26.65	−2.34	−2.73	−3.04	−3.25	−3.51	−3.65	−3.81
C_{3a}	38.96	28.89	−2.58	−2.97	−3.24	−3.42	−3.63	−3.74	−3.86
C_{3b}	29.67	28.43	−2.32	−2.75	−3.04	−3.23	−3.45	−3.58	−3.76
C_4	16.85	21.89	−3.05	−3.23	−3.38	−3.48	−3.60	−3.69	−3.81
C_{4a}	13.07	22.80	−3.31	−3.43	−3.53	−3.61	−3.70	−3.77	−3.86
C_{4b}	13.75	23.18	−3.03	−3.22	−3.36	−3.45	−3.56	−3.65	−3.78
C_5	4.92	19.62	−4.44	−4.52	−4.57	−4.61	−4.66	−4.72	−4.81
C_{5a}	2.47	18.80	−3.72	−3.72	−3.73	−3.74	−3.77	−3.80	−3.86
C_{5b}	2.20	19.04	−3.46	−3.54	−3.60	−3.63	−3.69	−3.74	−3.83
C_6	0.00	16.80	−2.97	−3.04	−3.09	−3.11	−3.16	−3.24	−3.54

[a] Enthalpy contributions are in kcal/mol. Entropy and heat capacity contributions are in cal/(mol K). Enthalpy and entropy are at standard conditions of 298.15 K, 1 bar. Si_a indicates a formally doubly bonded silicon atom (as in a silene). Si_b indicates a divalent silicon atom (as in a silylene). C_3, C_4, and C_5 are contributions of three-, four-, and five-membered rings, respectively. C_{3a}, C_{4a}, C_{5a} are rings containing a double bond. C_{3b}, C_{4b}, and C_{5b} are rings containing a divalent silicon atom.

membered ring. Group parameters for rings with more than five members could not be determined from the calculations of Katzer et al., since they only considered molecules with up to five silicon atoms. These rings should be nearly unstrained, so their group contribution to the heat of formation can be taken to be zero. However they do contribute to the entropy and heat capacity. To determine the entropy and heat capacity group values for the six-membered ring, we performed an ab initio geometry optimization and frequency calculation for cyclohexasilane at the Hartree−Fock level using the 6-31G(d) basis set. This calculation was carried out using Gaussian94.[47] The entropy and heat capacity were calculated from the standard expressions using the calculated vibrational frequencies scaled by the standard factor of 0.8929. The resulting entropy and heat capacity group contributions were used for all six-membered rings. No larger rings were considered in this work.

Since no groups were defined for adjacent silicon atoms with silylene (Si_b) or silene (Si_a) functionality, this scheme cannot be used for molecules containing such groups. Therefore, we have considered only those silylenes and silenes that can be formed by removal of a single pair of hydrogen atoms from the parent silane. Since formation of silylenes and silenes from silanes is substantially endothermic and endoergic for the conditions considered here, molecules with multiple silene or silylene groups are not expected to be formed in significant quantities. At sufficiently high temperatures, such species would presumably become important. For polycyclic molecules, the ring contributions were treated as additive. In an ab initio study of strain energies in silicon rings and clusters, Zhao and Gimarc[48] found that total ring strain in polycyclic structures was approximately equal to the sum of the strain energy of the individual rings. The ring strain energies for the individual silane and silene rings from our group additivity scheme agreed reasonably well with the values calculated by Zhao and Gimarc, as well as with those presented by Grev and Schaefer.[49] For hexasilaprismane (Si_6H_6 with two three-membered and three four-membered rings) and octasilacubane (Si_8H_8 with six four-membered rings), two extreme cases where the total strain is somewhat higher than predicted by additivity of the individual ring strains, our scheme predicts total strain energies that are, respectively, 4 and 10 kcal/mol lower than the values calculated by Zhao and Gimarc.

To further validate the group additivity scheme, ab initio molecular orbital calculations of the thermochemical properties of several larger clusters were carried out. Detailed results of these calculations will be presented elsewhere. Briefly, Gaussian94[47] was used to apply the CBS-4 method to several silicon hydride clusters. The CBS-4 method is one of the complete basis-set extrapolation methods developed by Petersson and co-workers.[50] Heats of formation of these polycyclic clusters (Si_nH_m) were calculated using the isodesmic reactions

$$Si_nH_{2m} + (2n - m)Si_2H_6 \rightarrow (2m - n)Si_3H_8 + 2(n - m)Si_4H_{10} \quad (3)$$

The heat of formation of the cluster (Si_nH_{2m}) was calculated using the known heats of formation of Si_2H_6, Si_3H_8, and Si_4H_{10} and the heat of reaction for eq 3 computed from the ab initio energies. The entropy and heat capacity were calculated from the moments of inertia and scaled vibrational frequencies computed at the HF/3-21G level. The results of these calculations are presented in Table 2. The ab initio based values agree well with those from group additivity for Si_8H_{12}, Si_9H_{14}, $Si_{10}H_{14}$, and $Si_{10}H_{16}$, which are all made up of five- and six-membered rings. There are significant discrepancies between the ab initio and group additivity values for the enthalpies of Si_6H_8, Si_7H_8, and Si_7H_{10}, which are made up of three- and four-membered rings. The calculations of Nagase et al.[51] showed that silyl substitution decreases the strain energy of small silicon hydride rings. Our group additivity scheme does not account for this

TABLE 2: Cluster Thermochemistry from ab Initio Calculations[a]

	ab initio			group additivity		
molecule	$\Delta H^\circ_{f,298}$	S°_{298}	$C_{p,298}$	$\Delta H^\circ_{f,298}$	S°_{298}	$C_{p,298}$
Si_6H_8	105.2	96.5	43.1	118.7	92.2	43.4
Si_7H_8	122.1	101.0	48.2	140.9	93.5	48.1
Si_7H_{10}	95.1	107.7	51.9	109.0	103.2	51.7
Si_8H_{12}	83.5	111.1	60.1	82.7	112.1	56.6
Si_9H_{14}	82.4	125.3	69.0	87.3	125.0	67.1
$Si_{10}H_{14}$	97.0	130.7	73.9	102.5	126.9	69.0
$Si_{10}H_{16}$	85.9	135.8	77.8	87.0	135.1	79.1

[a] Enthalpies in kcal/mol, entropies and heat capacities in cal/(mol K) at standard conditions of 298.15 K, 1 bar. Ab initio values calculated using isodesmic reactions as described in the text.

and, therefore, overestimates the enthalpy of formation for the compounds containing highly substituted three- and four-membered rings. With sufficient data, this could be remedied by introducing additional ring correction groups that take into account the substitution patterns on the ring, but we did not do so for this work.

A set of structures that were not adequately described by the group additivity scheme were bicyclo[1.1.1]pentasilane (Si_5H_8) and the species obtained by removing H_2 from it. These were not included in the fitting procedure. The group additivity method underpredicted the enthalpy of formation of bicyclo-[1.1.1]pentasilane and its silylene derivative, bicyclo[1.1.1]-pentasilan-2,2-diyl, by 5.5 and 4.5 kcal/mol relative to the calculations of Katzer et al.[42] We, therefore, used their reported thermodynamic properties for these two species in all subsequent calculations. Katzer et al.[42] did not report calculations for a silene analogue of this structure. They found that the most stable isomer of Si_5H_6 was the bicyclic diradical bicyclo[1.1.1]-pentasilan-1,3-diyl. Like the silenes, this species is expected to be unreactive, since it is highly stabilized relative to other radical species and would therefore not be likely to abstract hydrogen from other species. We used this diradical, with the thermochemistry calculated by Katzer et al., in place of the silene isomer of Si_5H_6. In kinetic calculations, we used the same reactivity rules for it that were used for the silenes. This is a reasonable approximation since this diradical is converted to a silylene by two H-atom migrations that are essentially the same as the H migration that converts a silene to a silylene. The group additivity scheme did not consider diradical species, and no diradicals other than Si_5H_6 were included in the thermodynamic and kinetic calculations presented here. For Si_4H_6, the 1,3-diradical was predicted by Katzer et al. to be about 2.5 kcal/mol lower in energy than the silene. This difference is comparable to the uncertainties in the group additivity calculations, and we simply used the silene isomer in our calculations. It appears that the diradical species are unusually stable when the radical centers are at opposite corners of a four-membered ring. Thus, they may also be more stable than the corresponding silene for some larger molecules with four-membered rings, such as compounds related to octasilacubane. However, a detailed consideration of those structures would go well beyond the scope of this work.

Since it would not be feasible to include all possible structural isomers in a kinetic description of clustering, we used the group additivity scheme presented above to identify the most stable isomer of each type (silane, silene, and silylene) for each stoichiometry (Si_nH_{2m}). These isomers and their calculated enthalpies of formation are presented in Figure 1. Here and throughout this work, we use the suffix A to denote silenes and B to denote silylenes, thus disilene (H_2SiSiH_2) is written as Si_2H_4A and silylsilylene (H_3SiSiH) is written as Si_2H_4B. For all species with three or more silicon atoms, except for the Si_5H_x species discussed above, the group additivity values of thermochemical parameters were used. For species with one or two silicon atoms, established values from the literature were used.[14,52,53] The THERM program[54] was used to implement the group additivity scheme, to manage the thermodynamic database, and to perform polynomial fits to the thermodynamic properties in the standard NASA format that is used in the CHEMKIN series of codes.[55] The CHEMKIN adaptation of the STANJAN code[56] was used for the calculations of equilibrium composition presented below.

We can obtain some preliminary insight into the clustering and nucleation process by looking at the thermochemistry of these clusters and the resulting equilibria. Figure 2 presents the equilibrium composition among the species shown in Figure 1, plus the smaller species Si_nH_{2m}, $n = 1$ or 2, and hydrogen or helium bath gas. Species not shown are present in concentrations below or only slightly above the lower limits of the plots. Note that these results do not represent the true equilibrium state of the system, but rather a partial equilibrium among these species with 10 or fewer silicon atoms. The true equilibrium state under all of these conditions is nearly complete conversion of silane to crystalline silicon and molecular hydrogen. Equilibrium calculations that included pure silicon clusters Si_n ($1 \le n \le 10$), using the same thermochemistry discussed in previous work,[34,52,57] predicted that the Si_7 cluster would be the dominant cluster present at partial equilibrium among the pure silicon clusters and the species shown in Figure 2. However, in the kinetic simulations presented below, formation of pure silicon clusters was found to be unimportant compared to formation of hydrogenated silicon clusters. While formation of pure silicon clusters is thermodynamically favorable under these conditions, it appears that the decomposition kinetics are such that they are not formed in significant quantities (see below). Therefore, it is the equilibrium among the hydrogenated clusters that is relevant to particle nucleation under conditions considered here, and that is what is presented in Figure 2.

The features that we would expect for the generalized overall clustering reaction

$$n\mathrm{SiH_4} \rightarrow \mathrm{Si}_n\mathrm{H}_{2m} + (2n - m)\mathrm{H_2} \qquad (4)$$

are observed in Figure 2. On the basis of reaction 4, we can write the equilibrium concentration of a given cluster in terms of the equilibrium concentrations of hydrogen and silane. Expressed in terms of mole fractions, this relationship is

$$X_{\mathrm{Si}_n\mathrm{H}_{2m,\mathrm{eq}}} = \frac{\exp(\Delta S^\circ/R - \Delta H^\circ/RT) X^n_{\mathrm{SiH}_{4,\mathrm{eq}}}}{X^{2n-m}_{\mathrm{H}_{2,\mathrm{eq}}} (p/p_o)^{n-m+1}} \qquad (5)$$

where $X_{\mathrm{Si}_n\mathrm{H}_{2m,\mathrm{eq}}}$, $X_{\mathrm{SiH}_{4,\mathrm{eq}}}$, and $X_{\mathrm{H}_{2,\mathrm{eq}}}$ are the equilibrium mole fractions of Si_nH_{2m}, SiH_4, and H_2; ΔS° and ΔH° are the standard entropy and enthalpy of reaction 4; p is the total pressure; and p_o is the reference pressure. Both the change in enthalpy and change in entropy for the overall process are positive. The increase in entropy is simply due to the increase in the number of moles of gaseous species. At sufficiently low temperatures, the enthalpic effect dominates and silane is more stable than the larger clusters. Conversely, at high temperatures, the entropic effect dominates and cluster formation is favored. As can be seen from eq 5, the equilibrium concentration of a given cluster increases with increasing silane mole fraction and decreases with increasing pressure or with hydrogen addition. In general, the

Name	Structure	$\Delta H_f°$	S°	Name	Structure	$\Delta H_f°$	S°	Name	Structure	$\Delta H_f°$	S°	Name	Structure	$\Delta H_f°$	S°
Si_3H_8		29.8	83.0	$Si_6H_{10}B$		114.9	109.3	Si_8H_{16}		72.4	140.3	Si_9H_{12}		128.8	117.9
Si_3H_6A		74.6	79.7	Si_6H_{10}		86.8	101.9	$Si_8H_{14}A$		116.7	136.8	$Si_9H_{10}A$		165.1	118.1
Si_3H_6B		86.3	81.4	Si_6H_8A		120.3	102.0	$Si_8H_{14}B$		125.1	140.4	$Si_9H_{10}B$		177.9	116.6
Si_3H_6		64.8	73.9	Si_6H_8B		138.6	100.9	Si_8H_{14}		82.0	128.8	Si_9H_{10}		141.5	103.5
Si_3H_4A		111.3	72.4	Si_6H_8		118.7	92.2	$Si_8H_{12}A$		118.2	125.5	Si_9H_8A		184.5	100.1
Si_3H_4B		115.9	73.7	Si_6H_6A		154.1	92.4	$Si_8H_{12}B$		134.2	126.0	Si_9H_8B		190.9	100.3
Si_4H_{10}		37.9	98.5	Si_6H_6B		167.8	90.9	Si_8H_{12}		82.7	112.1	$Si_{10}H_{22}$		87.23	188.2
Si_4H_8A		80.3	96.4	Si_6H_6		150.7	82.5	$Si_8H_{10}A$		118.9	108.7	$Si_{10}H_{20}A$		136.9	187.0
Si_4H_8B		91.6	96.6	Si_7H_{16}		62.6	143.4	$Si_8H_{10}B$		129.5	108.3	$Si_{10}H_{20}B$		141.0	186.2
Si_4H_8		55.0	84.9	$Si_7H_{14}A$		108.6	141.7	Si_8H_{10}		131.2	104.5	$Si_{10}H_{20}$		87.5	169.4
Si_4H_6A		95.5	82.2	$Si_7H_{14}B$		115.3	143.5	Si_8H_8A		167.5	104.7	$Si_{10}H_{18}A$		137.6	167.3
Si_4H_6B		109.6	84.2	Si_7H_{14}		65.3	126.7	Si_8H_8B		180.3	103.1	$Si_{10}H_{18}B$		141.4	169.2
Si_5H_{12}		45.0	112.1	$Si_7H_{12}A$		107.3	124.3	Si_8H_8		143.9	90.0	$Si_{10}H_{18}$		91.2	154.7
$Si_5H_{10}A$		87.9	112.4	$Si_7H_{12}B$		119.1	124.8	Si_9H_{20}		80.1	174.6	$Si_{10}H_{16}A$		132.3	152.9
$Si_5H_{10}B$		97.7	112.2	Si_7H_{12}		84.4	115.4	$Si_9H_{18}A$		122.0	174.3	$Si_{10}H_{16}B$		146.1	152.4
Si_5H_{10}		52.6	98.3	$Si_7H_{10}A$		119.2	113.7	$Si_9H_{18}B$		132.9	174.7	$Si_{10}H_{16}$		87.0	135.1
Si_5H_8A		94.5	94.0	$Si_7H_{10}B$		136.2	114.4	Si_9H_{18}		80.4	155.8	$Si_{10}H_{14}A$		130.7	132.5
Si_5H_8B		107.5	95.8	Si_7H_{10}		109.0	103.2	$Si_9H_{16}A$		124.7	152.3	$Si_{10}H_{14}B$		139.2	132.5
Si_5H_8		82.7	85.7	Si_7H_8A		144.4	103.3	$Si_9H_{16}B$		133.2	155.9	$Si_{10}H_{14}$		102.5	126.9
Si_5H_6A		103.8	84.3	Si_7H_8B		158.1	101.8	Si_9H_{16}		86.6	141.7	$Si_{10}H_{12}A$		140.6	123.6
Si_5H_6B		127.6	87.1	Si_7H_8		140.9	93.5	$Si_9H_{14}A$		125.2	139.2	$Si_{10}H_{12}B$		149.3	123.1
Si_6H_{14}		54.5	127.9	Si_7H_6A		177.2	93.7	$Si_9H_{14}B$		138.8	138.9	$Si_{10}H_{12}$		139.1	117.0
$Si_6H_{12}A$		102.9	128.0	Si_7H_6B		190.0	92.1	Si_9H_{14}		87.3	125.0	$Si_{10}H_{10}A$		176.3	117.2
$Si_6H_{12}B$		107.3	128.0	Si_8H_{18}		69.6	157.0	$Si_9H_{12}A$		123.5	121.7	$Si_{10}H_{10}B$		188.5	113.7
Si_6H_{12}		57.2	111.2	$Si_8H_{16}A$		112.9	160.0	$Si_9H_{12}B$		136.8	121.8	$Si_{10}H_{10}$		163.7	104.8
$Si_6H_{10}A$		101.5	107.7	$Si_8H_{16}B$		122.4	157.1								

Figure 1. Heat of formation (kcal/mol) and standard entropy (cal/(mol K)) at 298.15 K, 1 bar, of silicon hydrides considered in this work. The structures shown are believed to be the most stable isomer for each stoichiometry and species type. Species suffixed with A are silenes (except Si_5H_6A, which is a diradical), and species suffixed with B are silylenes. The enthalpies and entropies are from the group additivity scheme described in the text, except Si_5H_8, Si_5H_6A, and Si_5H_6B for which the values from Katzer et al.[42] were used directly.

effects of hydrogen and silane concentrations are relatively strong, while the effect of pressure is relatively weak.

For the conditions of Figure 2a, corresponding to 1% SiH_4 in helium at 1 atm total pressure, significant clustering occurs over the entire temperature range shown. There is a shift from the more hydrogenated clusters Si_8H_{12}, $Si_{10}H_{16}$, and $Si_{10}H_{14}$ at low temperatures to smaller and less hydrogenated species at higher temperatures. This shift is due to the higher overall entropy of reaction when less hydrogenated species are produced. Figure 2b shows results at the same total pressure as Figure 2a, but with the He bath gas replaced by H_2. This shows strong suppression of clustering by hydrogen, which is also what is observed experimentally.[36] The equilibrium conversion of silane to clusters is at most a few percent over the entire temperature range shown. Figure 2c shows the dependence of the equilibrium cluster mole fractions on the initial silane concentration in helium at fixed temperature and pressure. At this temperature, most of the silane is converted to larger clusters for all of the initial silane concentrations shown. With increasing silane fraction, there is a shift from the less hydrogenated to more hydrogenated clusters. Figure 2d shows the dependence of the equilibrium cluster mole fractions on initial silane concentration in hydrogen for fixed temperature and pressure. Note the very strong dependence of cluster formation on the initial silane concentration and the sharp onset of formation of $Si_{10}H_{14}$ at around 3% silane in H_2. This is consistent with what is observed experimentally[36] and is what we would expect based on reaction 4 and eq 5.

III. Clustering Reaction Mechanism and Kinetics

On the basis of the thermochemical properties presented in Figure 1 and the known reactivity of the small silicon hydrides, we constructed a large reaction mechanism for cluster formation

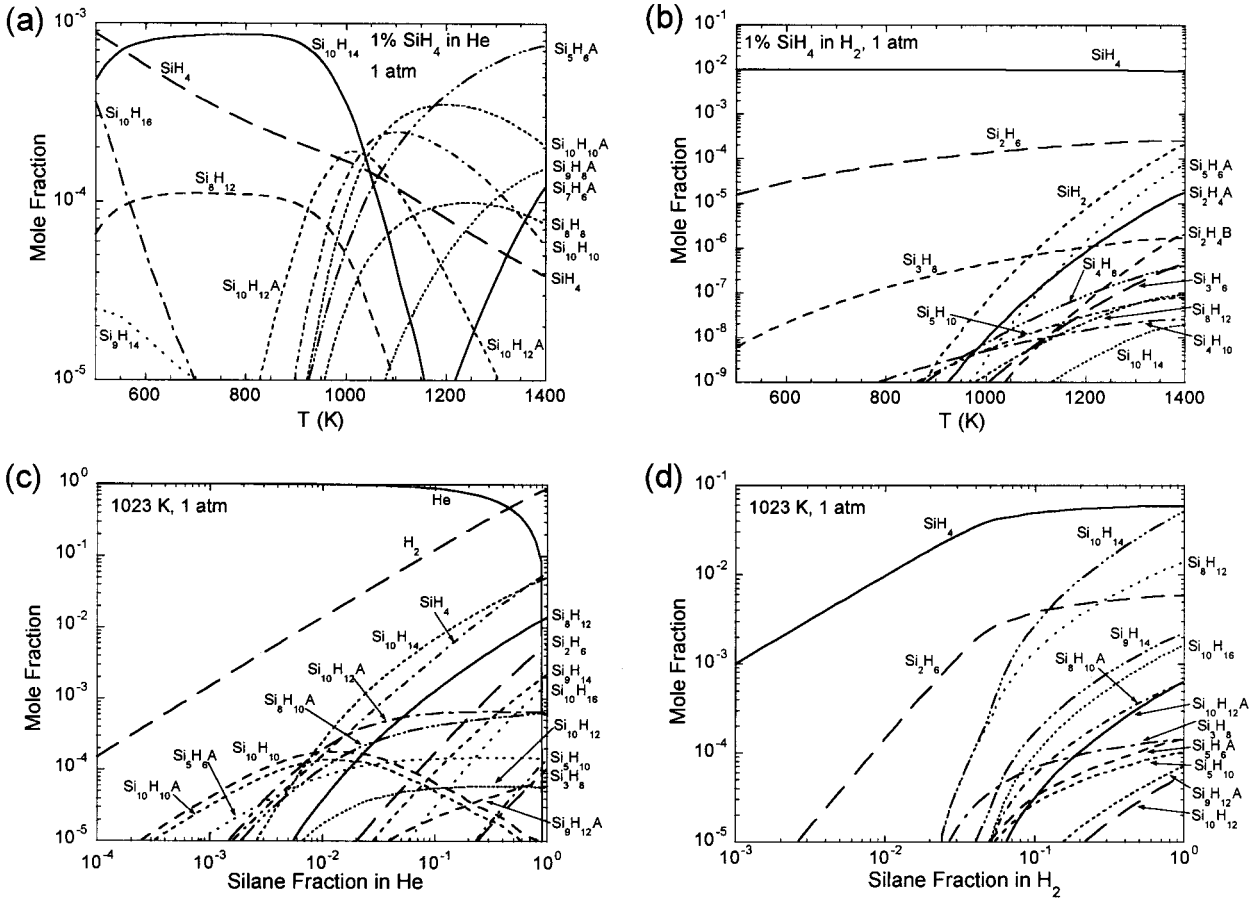

Figure 2. Mole fractions of the most abundant species at equilibrium among the species shown in Figure 1 plus SiH_2, SiH_4, Si_2H_4A, Si_2H_4B, and Si_2H_6. (a) variation of equilibrium composition with temperature at 1 atm and an initial composition of 1% SiH_4 in He. (b) Variation of equilibrium composition with temperature at 1 atm and an initial composition of 1% SiH_4 in H_2. (c) Variation of equilibrium composition with initial silane fraction in He at 1023 K and 1 atm. (d) Variation of equilibrium composition with initial silane concentration in H_2 at 1023 K and 1 atm.

TABLE 3: Reaction Types and Reactivity Rules[a]

reaction type	prototypical reactions	general form	preexponential factor (s^{-1})	activation energy
H_2 elimination from a silane	$SiH_4 \leftrightarrow SiH_2 + H_2$ $Si_2H_6 \leftrightarrow Si_2H_4B + H_2$	$Si_nH_{2m} \leftrightarrow Si_nH_{2(m-1)} + H_2$	2×10^{15}	$\Delta H_{rxn,1000}$
silylene elimination from a silane	$Si_2H_6 \leftrightarrow SiH_2 + SiH_4$ $Si_3H_8 \leftrightarrow Si_2H_4B + SiH_4$	$Si_nH_{2m} \leftrightarrow Si_lH_{2k}B + Si_{n-l}H_{2(m-k)}$	2×10^{15}	$\Delta H_{rxn,1000}$
silylene elimination from a silene	$Si_3H_6A \leftrightarrow SiH_2 + Si_2H_4A$ $Si_4H_8A \leftrightarrow Si_2H_4B + Si_2H_4A$	$Si_nH_{2m}A \leftrightarrow Si_lH_{2k}B + Si_{n-l}H_{2(m-k)}A$	2×10^{15}	$\Delta H_{rxn,1000}$
silylene to silene isomerization	$Si_2H_4B \leftrightarrow Si_2H_4A$ $Si_3H_6B \leftrightarrow Si_3H_6A$	$Si_nH_{2m}B \leftrightarrow Si_nH_{2m}A$	1×10^{13}	7.5 kcal/mol
ring opening	$Si_3H_6 \leftrightarrow Si_3H_6B$ $Si_4H_8 \leftrightarrow Si_4H_8B$	$Si_nH_{2m} \leftrightarrow Si_nH_{2m}B$	2×10^{15}	$\Delta H_{rxn,1000}$

[a] Molecules without a suffix are fully saturated silanes. Molecules with an A suffix are silenes. Molecules with a B suffix are silylenes. No special notation is used to differentiate between acyclic, cyclic, and polycyclic molecules. $\Delta H_{rxn,1000}$ is the enthalpy of reaction at 1000 K. The reverse rate constants were computed from the forward rate constants and equilibrium constants.

during thermal decomposition of silane. As a base reaction mechanism, we used the reactions and rate parameters presented by Ho et al.[58] for reactions among species containing one or two silicon atoms (Si, SiH_2, SiH_4, Si_2H_4A, Si_2H_4B, Si_2H_6). This mechanism explicitly treats the pressure dependence of the unimolecular decomposition and recombination reactions. It is the most complete and thoroughly validated of the detailed mechanisms for silane decomposition that have been presented in the literature. For the larger silicon hydride species, five types of reversible chemical reactions were considered. These reactions and the rules used for estimating their rate parameters are presented in Table 3. The complete reaction mechanism included all of the possible reactions of these five types for which all of the participating species were among those shown in Figure 1 or the smaller compounds of the same types (SiH_4, SiH_2, Si_2H_6, Si_2H_4A, and Si_2H_4B). Note that SiH_2 participates in these reactions as a silylene (species of type B). Further dehydrogenation to give species with higher Si to H ratios than those presented in Figure 1 was not included.

A parallel path for cluster formation from silicon atoms via the reversible reactions $Si_i + Si \leftrightarrow Si_{i+1}$ ($1 \le i \le 10$, with the reaction taken to be irreversible for $i = 10$) was included to assess the potential importance of homogeneous nucleation of pure silicon from its vapor. Rate parameters for these reactions and the thermochemistry of the pure silicon clusters were essentially the same as those presented in previous work.[34] Hydrogenation of these clusters was not included. Therefore, this pure silicon nucleation pathway did not interact directly

with the nucleation pathway involving the hydrogenated silicon clusters. For all of the conditions considered here, the pure silicon clustering path made a negligible contribution to particle nucleation, although at sufficiently high temperatures one would expect it to become important.

Hydrogenated clusters with 11−20 silicon atoms were assumed to form irreversibly by reactions of the same types as those in Table 3. These were the reactions

$$Si_nH_{2m} + Si_lH_{2k}B \rightarrow Si_{n+l}H_{2(m+k)} \quad (5)$$

and

$$Si_nH_{2m}A + Si_lH_{2k}B \rightarrow Si_{n+l}H_{2(m+k)} \quad (6)$$

Both of these reaction types were assumed to occur at the gas-kinetic collision rate of the reactants. Including all of the reactions described above gave a total of 2614 reactions among 221 species. Obviously, only a small fraction of the reactions and species are important under any given set of conditions, but it is difficult to identify a priori which reactions can safely be excluded. Therefore, the results presented below are based on this full set of reactions.

A brief explanation and justification for the selection of the reactions and rate-parameter estimation rules given in Table 3 is now presented. It has been well-established experimentally[10,12,22] and theoretically[17−19] that the characteristic thermal decomposition reactions of silicon hydrides are elimination reactions that produce a silylene and a silane or a silylene and hydrogen. Likewise, the characteristic reactions of silylenes are known to be insertion into Si−H bonds and insertion into H_2[13,20] to produce a silane. These eliminations and insertions are the reverse of one another, and their rate parameters are related via microscopic reversibility. Insertion reactions of SiH_2 with H_2, SiH_4, Si_2H_6, and Si_3H_8 all have small negative activation energies and rate parameters close to the collision rate (in the high-pressure limit), indicating that they are barrierless processes.[20] Insertion reactions of larger silylenes have not been studied experimentally, but ab initio molecular orbital studies[59] of the insertion of silylsilylene (Si_2H_4B) into hydrogen indicate that it also occurs without a barrier. Substituents on the silylene such as fluorine, chlorine, and methyl that are more electronegative than silicon are known to slow insertion reactions of the silylene with Si−H bonds and H_2,[13] but silyl substituents are expected to have little effect. Since these insertions are all barrierless, the corresponding eliminations (the reverse reactions) are expected to have activation energies that are approximately equal to the enthalpy of reaction. This has been confirmed by experimental[8,9,14,22,26] and theoretical[14,17−19,59] studies of the thermal decomposition of SiH_4, Si_2H_6, Si_3H_8, and Si_4H_{10}. It has been shown[17] that hydrogen elimination from disilane (and by analogy from larger polysilanes) occurs exclusively as a 1,1-elimination. The barrier for 1,2-elimination is substantially higher than that for the 1,1-elimination.

All of the elimination reactions occur via a three-centered transition state and have very similar entropies of activation. Therefore, we use the same preexponential factor (2×10^{15} s^{-1}) for all of the elimination reactions and set the activation energy for these reactions equal to the enthalpy of reaction at 1000 K. The preexponential value was simply chosen by comparison to that for silane and disilane decomposition. Rate parameters for the insertion reactions are computed from the elimination rate parameters and the equilibrium constant. In addition to all possible silylene and hydrogen eliminations from silanes, we also include silylene eliminations from silenes. Rate parameters for these eliminations were estimated in the same way as those for silylene elimination from silanes. The corresponding insertion reaction becomes important under conditions where concentrations of certain silenes become comparable to the concentrations of the silanes (see below). There is neither experimental nor theoretical information on intramolecular insertion reactions that produce a ring. However, it is reasonable to assume that the reactivity of the divalent silicon atom in a silylene with Si−H bonds in the same molecule is no different than its reactivity with Si−H bonds in other molecules. Of course, the overall energetics of such a reaction are influenced by the strain energy of the ring that is formed. We have included these intramolecular insertions, with the rate parameters for the corresponding elimination reactions (ring-opening reactions) estimated in the same way as for the other eliminations.

Finally, we have included reversible isomerization of silylenes to silenes. For all of the silicon hydrides considered here, the silene is more stable than the silylene. The silenes are assumed to be unreactive with silanes and hydrogen. The silylenes and silenes are related by a 1,2-hydrogen migration. This has only been studied theoretically and only for the simplest reaction, silylsilylene (Si_2H_4B) isomerization to disilene (Si_2H_4A). The highest level ab initio calculations for this reaction[21] locate the barrier to reaction 7.5 kcal/mol above the silylsilylene isomer. We, therefore, use this value for the activation energy for all of the silylene to silene isomerizations. A preexponential factor of 10^{13} is used for all of these reactions. This is a typical value consistent with the tight, three-centered transition state for the H-migration reaction. At temperatures sufficiently high for significant silane pyrolysis to take place, these isomerization reactions will be much faster than any of the other reactions in the mechanism. Therefore, they are almost always in equilibrium, and our results are insensitive to the rate parameters used for these isomerization reactions.

A major simplification in this description of the chemistry is the inclusion of just one isomer of each type (silane, silylene, silene) for each stoichiometry. This is equivalent to the assumption that rearrangements to form the most stable isomer are infinitely fast. In some cases, this is clearly an imperfect assumption. For example, the reaction $Si_3H_6 + Si_3H_4B \leftrightarrow Si_6H_{10}$ requires substantial rearrangement of the initial product to reach the most stable isomer of Si_6H_{10}. However, under most conditions, reactions involving SiH_4 or SiH_2 dominate. For these reactions, the rearrangement to give the most stable isomer is simpler, typically just involving opening of a ring followed by formation of a larger, less strained ring. An example of this is $Si_4H_6B + SiH_4 \leftrightarrow Si_5H_{10}$. The silylcyclotetrasilane produced by the elementary insertion reaction is converted to cyclopentasilane by a simple ring opening and closing to form the larger ring. Ideally, one would treat all of these elementary steps separately and include all of the isomers produced. However, this is not feasible because of the large increase in the number of chemical species that would result. It may be possible to use automated mechanism generation, combined with production-rate-based criteria for inclusion of new chemical species,[60] to avoid this exponential growth in the number of chemical species. This approach will be pursued in continuing development of this mechanism.

Even with this simplification, the current mechanism contains far more chemical information than any previous description of silicon hydride clustering. This is the first model to include both growth and dehydrogenation via ring formation. We also capture the effects of ring strain, substitution patterns, and other structural features on the thermodynamics and kinetics of

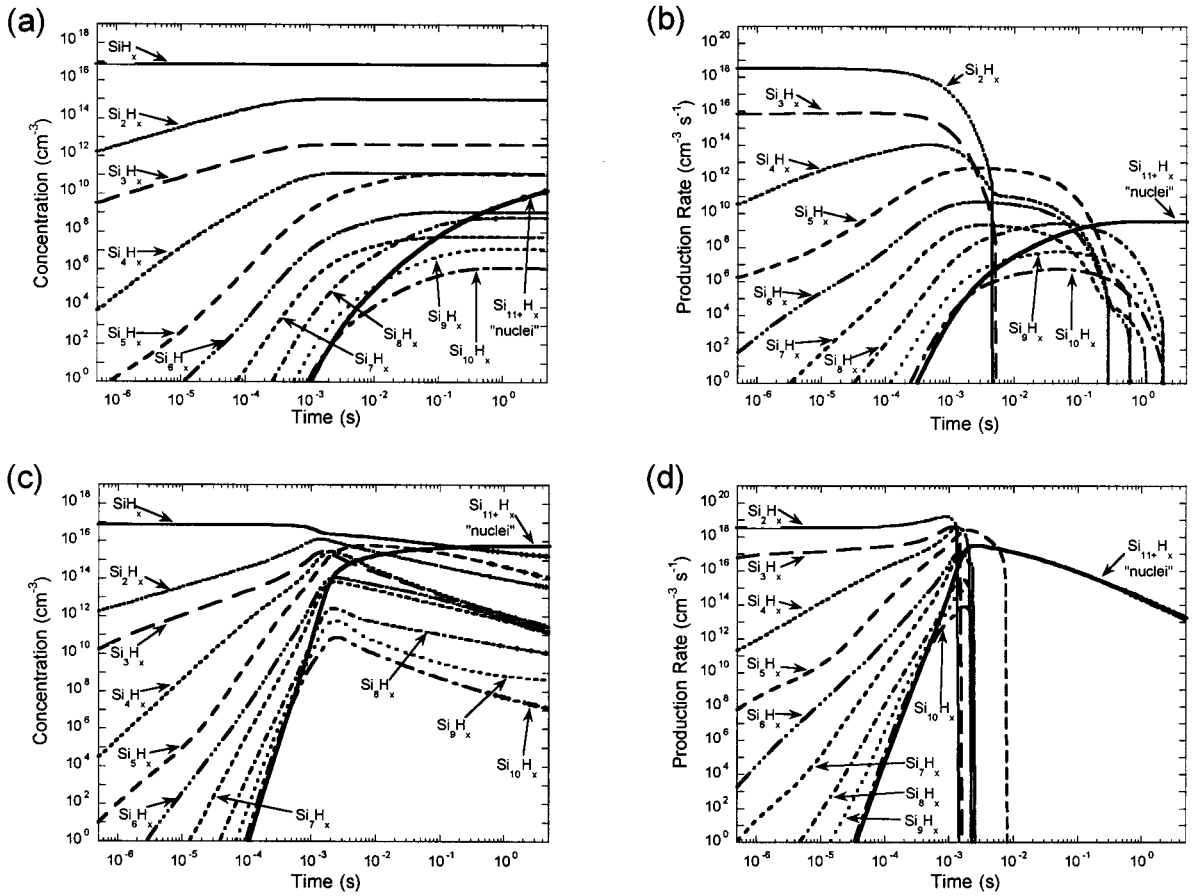

Figure 3. Predicted temporal profiles of total concentration and net production rate of silicon hydride clusters containing a given number of silicon atoms. Parts a and b are at 1023 K, 1 atm total pressure, and an initial composition of 1% silane in H_2. Parts c and d are for the same conditions with an initial composition of 1% silane in helium.

clustering. This represents a significant advance over previous models that included only linear polysilanes and used equal rate parameters for all of the growth reactions.[28,29]

IV. Kinetic Simulations and Reaction-Path Analysis

The reaction mechanism described above was used to simulate silane pyrolysis in a batch reactor with no surface reactions. Starting with some initial concentration of silane, the rate equations describing the evolution of species concentrations at fixed temperature and pressure were integrated to give species concentrations, species production rates, and reaction rates as a function of time. The SENKIN[61] program from the CHEMKIN family of codes was used to carry out this integration. Figure 3 shows the results of these simulations for two cases corresponding to only slight silane depletion (Figure 3 (a and b)) and substantial silane depletion (Figure 3 (c and d)) on the time scale considered. Concentrations of all clusters with a given number of silicon atoms have been summed and plotted as a single line. The clusters with 11 or more silicon atoms, which are assumed to form irreversibly, were summed to give the single curve labeled "nuclei".

In Figure 3a, the concentration of SiH_4 remains nearly constant at its initial value of 1% (in H_2). The larger species are present in substantially smaller concentrations throughout the range of times considered. The cluster concentrations increase monotonically to values that remain nearly constant at long times. As can be seen in Figure 3b, the net production rate of each size drops to zero (or a small negative value, not shown on the logarithmic scale) at a characteristic time. For Si_2H_x and Si_3H_x this time is around 5 ms. For Si_8H_x, Si_9H_x, and $Si_{10}H_x$, this time is about 2 s. For species with seven or fewer silicon atoms, the constant concentrations at long times are approximately equal to the concentrations that would be obtained from partial equilibrium calculations such as those shown in Figure 2. However, the total concentrations of species containing 8, 9, or 10 silicon atoms are 1−3 orders of magnitude below the values that would be obtained from partial equilibrium calculations. The absolute concentrations decrease with increasing cluster size, except for species containing five or eight silicon atoms. Examination of the cluster free energies shows that the Si_8H_{12} and Si_5H_6A isomers are unusually stable relative to the other clusters, although as noted above the group additivity may be substantially overestimating the heats of formation for some of the Si_6H_x and Si_7H_x clusters. For times longer than a few tenths of a second, the rate of production of nuclei (clusters with 11 or more silicon atoms) is nearly constant. This regime corresponds to steady-state nucleation. It is important to note that the present model does not account for additional reactions of the nuclei with each other (coagulation) or with smaller silicon hydrides (growth of the nuclei by surface reactions). These would be included in an aerosol dynamics model to which the kinetic model presented here could be coupled. This would, on a time scale which is not readily determined a priori, result in depletion of the gas-phase silicon hydrides due to surface reactions on particles which would, in turn, disturb the steady-state nucleation.

Figure 3c shows the results for the same temperature, pressure, and silane concentration as in Figure 3a, but with helium rather than H_2 as the bath gas. In this case, the silane is substantially depleted on the time scale shown. The majority

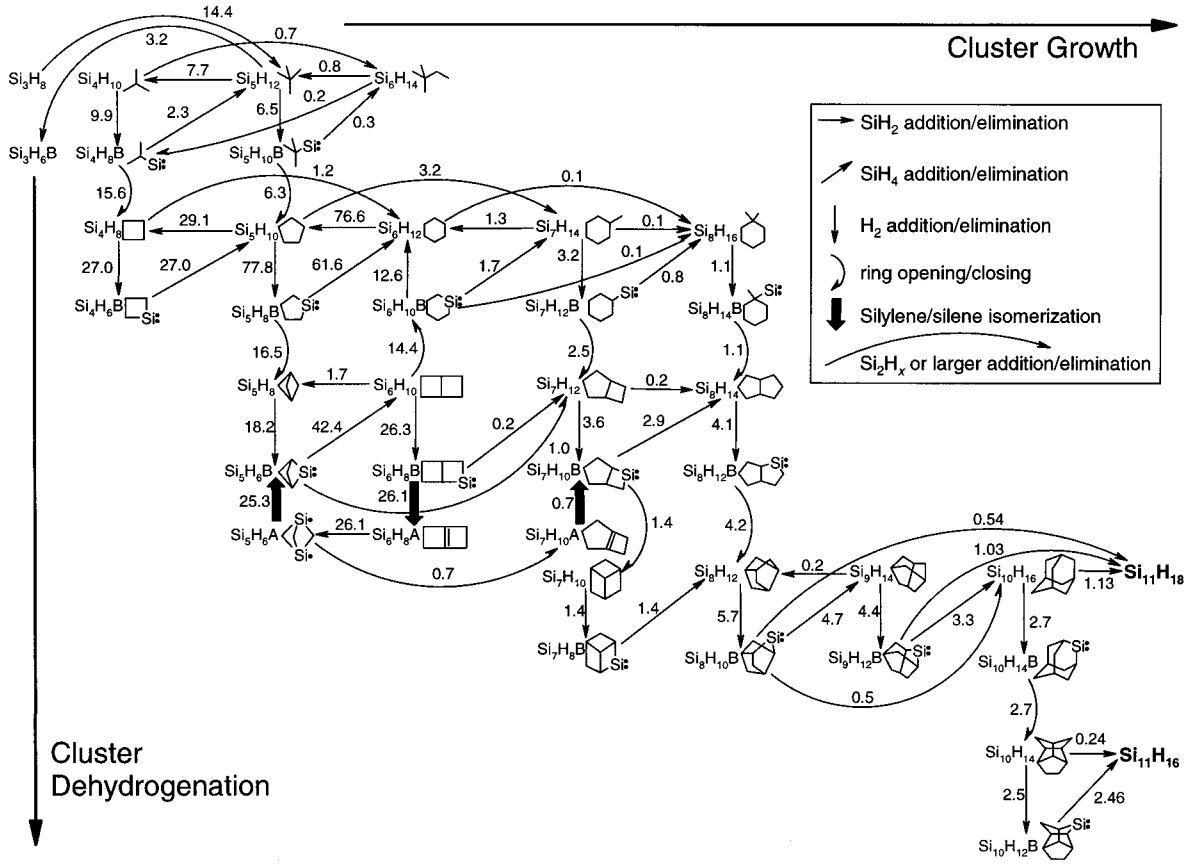

Figure 4. Diagram of dominant clustering pathways for 1% silane in H_2 at 1023 K, 1 atm, and a reaction time of 5 s. Numbers next to the arrows indicate net reaction rate in units of 10^{-15} mol/(cm^3 s).

of the silane is converted to larger species on a time scale of about 1 ms. At and just after this time, the concentrations of species with 2−10 silicon atoms go through clear maxima and then decrease monotonically as they are irreversibly converted to nuclei. The times at which their net production rates become negative can be seen in Figure 3d. This time is between 1 and 3 ms for all of the sizes except Si_5H_x, which has a positive net production for about 8 ms. For times longer than about 5 ms, Si_5H_x is the most abundant cluster size other than silane. The nucleation rate never reaches a constant value but goes through a maximum at about 3 ms, after which it decreases due to depletion of the silane precursor. The species concentration profiles for this case are not easily related to their concentrations at partial equilibrium.

The results presented in Figure 3 give an overview of the predicted clustering behavior, but we can obtain additional insights into the clustering process by considering the rates of individual reaction steps in more detail and identifying the dominant paths leading to formation of nuclei under different conditions. In Figures 4−7, we present reaction-path diagrams illustrating the dominant reactions that lead to chemical nucleation of particles. In each case, the species involved are arranged such that each column consists of species with the same number of silicon atoms, with the cluster size increasing from left to right. Each row consists of species of a given type (silane, silylene, or silene). The hydrogen-to-silicon ratio decreases and the number of rings in the cluster increases from the top to the bottom of the diagram. The species are connected by arrows of various types that indicate the different reaction types considered in this study, and the numbers next to the arrows indicate the net reaction rates. We have found these diagrams helpful in identifying the critical reaction paths and in understanding the nucleation process.

Figure 4 illustrates the dominant reaction pathways leading to cluster formation at a reaction time of 5 s for 1% silane in H_2 at the conditions of Figure 3a. The total nucleation rate is 5.6×10^{-15} mol/(cm^3 s), and 96% of that total occurs by the paths shown in Figure 4. The SiH_4 depletion rate is almost exactly 11 times the nucleation rate, and the rate of change of concentration of all species other than SiH_4 and the $Si_{11}H_x$ "nuclei" is much smaller. This indicates that steady-state nucleation is occurring from an effectively infinite pool of SiH_4. Figure 4 shows that for some cluster sizes, particularly Si_5H_x through Si_7H_x, growth occurs by several parallel reaction paths that make comparable contributions. However, when a cluster size of eight silicon atoms is reached, all of the paths converge at the unusually stable molecule Si_8H_{12}, which eliminates H_2 to give $Si_8H_{10}B$. As noted above, there is a kinetic bottleneck for growth from clusters containing seven silicon atoms to those containing eight silicon atoms. This is shown by the fact that all of the clusters with seven or fewer silicon atoms are in partial equilibrium with each other, while clusters with 8, 9, or 10 silicon atoms are present in concentrations substantially below what their concentrations would be if they were in equilibrium with the smaller clusters and silane.

Figure 5 shows the dominant reaction paths under the same conditions as in Figure 4 but at a much shorter time ($t = 0.5$ ms). At this time, the nucleation rate is still quite small, 9.4×10^{-23} mol/(cm^3 s). There are no cluster sizes for which all clusters are in steady state (net production rate near zero), although many individual species are in steady state. Since all of the cluster sizes are accumulating, reaction rates among the

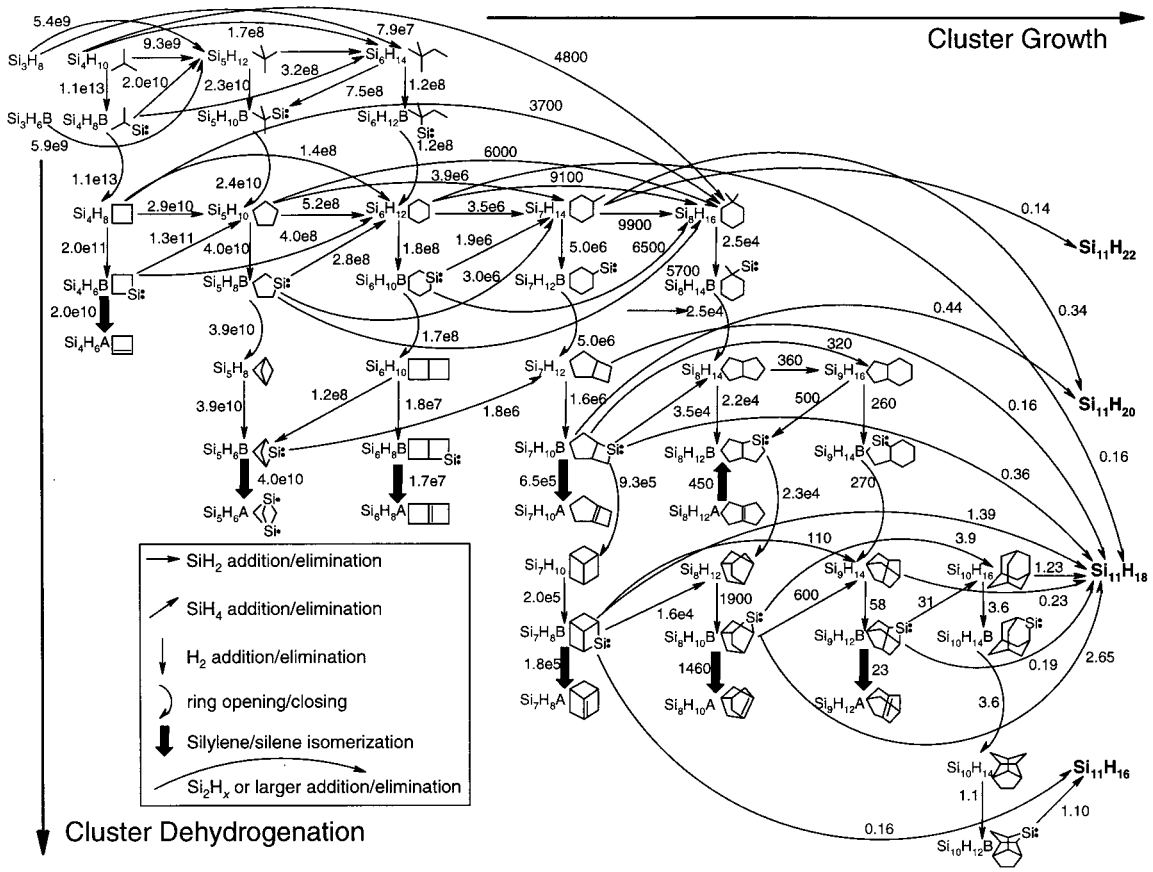

Figure 5. Diagram of dominant clustering pathways for 1% silane in H_2 at 1023 K, 1 atm, and a reaction time of 0.5 ms. Numbers next to the arrows indicate net reaction rate in units of 10^{-23} mol/(cm^3 s).

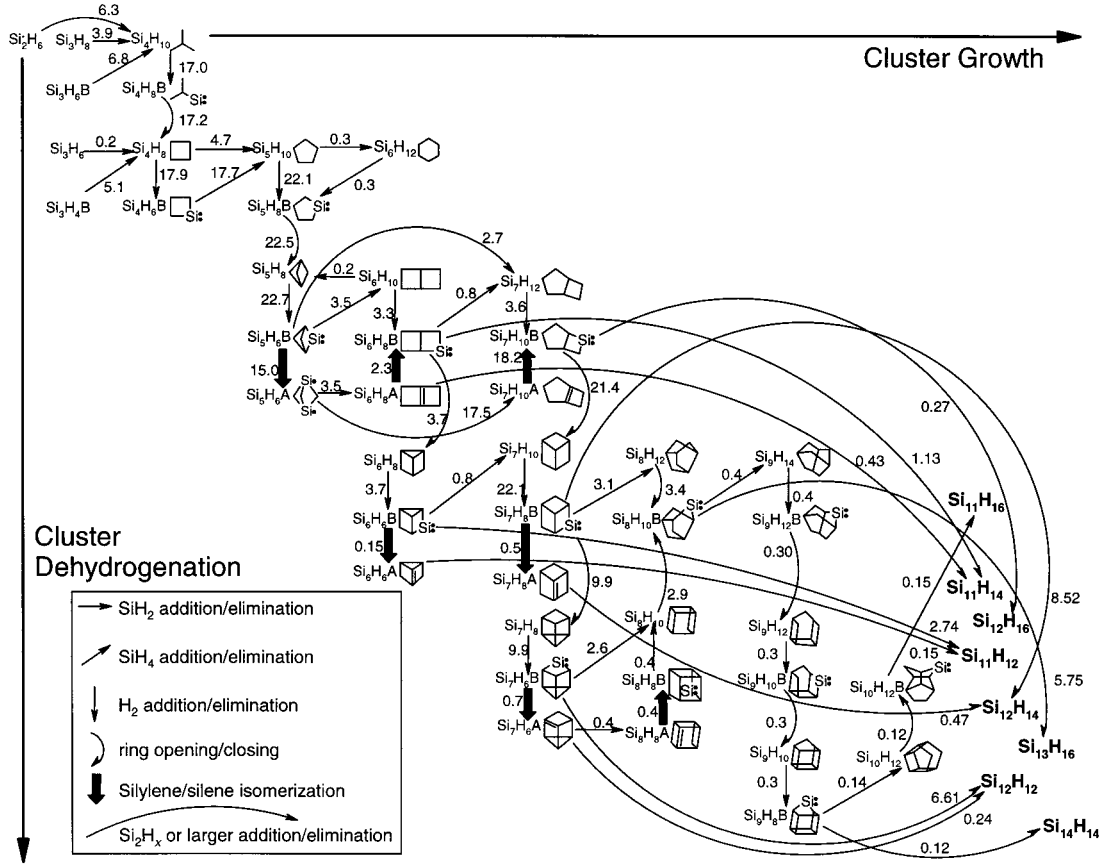

Figure 6. Diagram of dominant clustering pathways for 1% silane in helium at 1023 K, 1 atm, and a reaction time of 5 s. Numbers next to the arrows indicate net reaction rate in units of 10^{-12} mol/(cm^3 s).

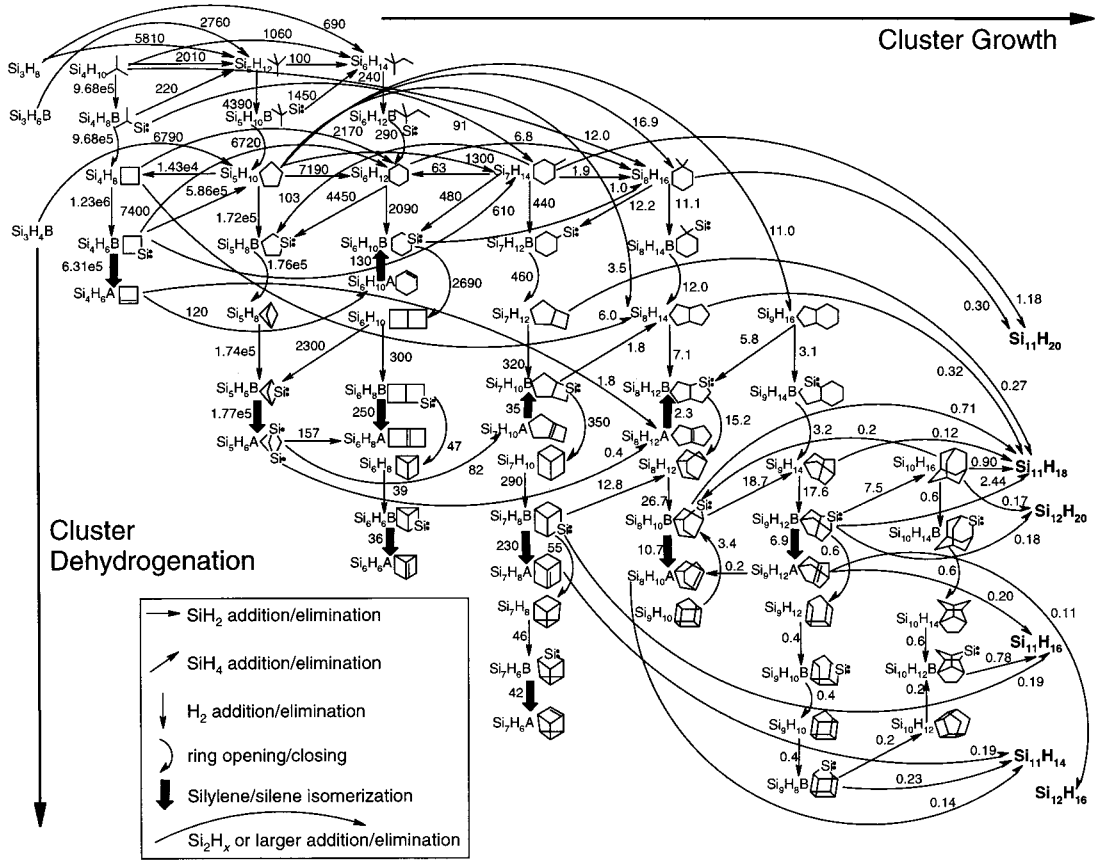

Figure 7. Diagram of dominant clustering pathways for 1% silane in helium at 1023 K, 1 atm, and a reaction time of 0.5 ms. Numbers next to the arrows indicate net reaction rate in units of 10^{-13} mol/(cm^3 s).

smaller species are much higher than the nucleation rate. This contrasts with the steady-state nucleation shown in Figure 4, where all of the reaction rates are of the same order of magnitude. At short times, there are substantially more reaction paths that contribute to cluster growth than during steady-state nucleation. Reactions involving jumps of several cluster sizes in a single step are much more important than they are at longer times, when reactions with SiH_4 and SiH_2 become dominant. Large species, particularly Si_8H_{16}, are formed in comparable amounts from several different smaller clusters. The majority of the nucleation flux still proceeds through Si_8H_{12}, although this path is not as dominant as it becomes at longer times.

Figure 6 shows the principle reaction paths for 1% silane in a helium bath gas, corresponding to the conditions of Figure 3c, after a reaction time of 5 s. At these conditions and reaction time, a substantial amount of Si_5H_6A is present and the most important contributions to nucleation come from reactions involving this species or its isomer Si_5H_6B. The total nucleation rate is 2.7×10^{-11} mol/(cm^3 s), with 98% of the total occurring by the paths shown. Analysis of the production and consumption rates of the species shows that they are all essentially in steady state except for SiH_4, Si_2H_6, Si_5H_6A, and the "nuclei". These conditions correspond to steady-state nucleation from a reservoir of SiH_4, Si_2H_6, and Si_5H_6A. On a per silicon atom basis, nuclei formation is about 48% from SiH_4, 48% from Si_5H_6A, and 4% from Si_2H_6. In this case, the majority of the nucleation flux does not go through Si_8H_{12} but rather comes from reactions of Si_6H_x and Si_7H_x species with Si_5H_6A and Si_5H_6B.

Finally, Figure 7 shows the dominant reaction paths for 1% silane in helium at a reaction time of 0.5 ms. As can be seen in Figure 3c, this time is slightly before the cluster concentrations reach their maximum values. The total nucleation rate is 9.8×10^{-13} mol/(cm^3 s), and 86% of that total occurs via the paths shown in Figure 7. There are many species whose concentrations are not in steady state, and production rates of species containing two or more silicon atoms are generally zero or positive. Substantial nucleation occurs from reactions of clusters containing 7, 8, 9, or 10 silicon atoms. While the majority of the nucleation flux does pass through Si_8H_{12}, there is also substantial formation of "nuclei" by reaction of Si_7H_x species with Si_4H_x species. This avoids the kinetic bottleneck associated with growth from clusters containing seven silicon atoms to larger sizes. Note that there is negligible production of clusters with 9 or 10 silicon atoms from the seven-silicon-atom clusters.

The results presented in Figures 4−7 show that, for given conditions, dominant pathways leading to chemical nucleation of particles can be identified. It is clear that the dominant reaction paths depend both on reaction conditions and reaction time. The reaction-time dependence presumably translates into a spatial dependence in an imperfectly mixed reactor operating at steady state. The dominant reaction paths are related to the relative thermodynamic stabilities of the species, as evidenced by the observation that the unusually stable species Si_5H_6A and Si_8H_{12} play special roles in the nucleation process. Under some conditions, the nucleation rate is established by a kinetic bottleneck for growth from clusters containing seven silicon atoms to clusters containing eight silicon atoms. There are other kinetic bottlenecks at smaller cluster sizes that are evident at short reaction times. For example, under the conditions of Figure 3a and b, partial equilibrium is established among the one-, two-, and three-silicon-containing molecules after about 5 ms. Between that time and a time of about 0.3 s, when a partial equilibrium with the four-silicon-containing clusters is established, the growth step from three to four silicon atoms acts as

a rate-limiting kinetic bottleneck. At longer times, the rate-limiting step shifts to larger sizes until it ends up at the step leading from seven-silicon to eight-silicon clusters. It is possible that additional kinetic bottlenecks occur at larger cluster sizes. For example, one might expect the $Si_{20}H_{20}$ isomer, in which the silicon atoms are arranged in an icosahedral structure, to have unusual stability, and therefore, there may be a bottleneck associated with its build-up to an equilibrium concentration in the same way that there is a bottleneck associated with the build-up of Si_8H_{12}. However, it would not be practical to continue increasing the largest cluster size considered in the model indefinitely. Since there may be additional bottlenecks at larger sizes, the nucleation rate predicted by this mechanism must be considered to be an upper limit, within the assumptions of the mechanism. Comparison of simulations using the mechanism presented here to one that was terminated by irreversible formation of six-silicon-containing clusters showed that qualitatively the same behavior, including temperature and pressure dependence of the nucleation rate, was predicted by both mechanisms. However, the absolute value of the predicted nucleation rate is several orders of magnitude smaller for the current mechanism than for the smaller mechanism. This is simply a result of the additional kinetic bottlenecks that occur at cluster sizes not included in the smaller mechanism.

Growth of linear or branched acyclic clusters was found to be negligible under all of the conditions examined, including those where H_2 was present in large excess. This mechanism predicts that the clusters formed have fairly compact polycyclic structures. For clusters with eight or more silicon atoms, the most abundant structures are those made up of five- and six-membered rings. The dominant eight-silicon cluster, Si_8H_{12}, is made up entirely of five-membered rings, with four bridgehead atoms that are each members of three rings. The most abundant nine-silicon cluster, Si_9H_{14}, can be obtained from the Si_8H_{12} structure by insertion of silylene into a bond connecting two of the bridgehead atoms. This expands two of the five-membered rings to six-membered rings. Repeating this process at the other bond connecting two bridgehead atoms gives the $Si_{10}H_{16}$ isomer, the silicon analogue of adamantane. This compound is made up entirely of six-membered rings and can be viewed as the smallest molecular analogue of the diamond cubic structure of bulk silicon, since its atoms are essentially in the lattice positions of that structure. Another abundant 10-silicon isomer, $Si_{10}H_{14}$, can be obtained directly from Si_8H_{12} by adding Si_2H_4 across two nonbridgehead atoms to create an additional five-membered ring. The structure of these clusters suggests that continued growth will lead to particles that have compact structures made up of five- and six-membered rings, with hydrogen present only at the surface of the clusters. This is consistent with the relatively low degree of hydrogenation of the silicon particles studies by Onischuk et al.[40]

It would be useful, for purposes of modeling aerosol dynamics in real reactors, to have a simpler and computationally less expensive means of computing the nucleation rate than is provided by a large, detailed reaction mechanism. From the results presented above, it is clear that there are some regimes where simple, approximate expressions for the nucleation rate can be derived. One such case is the conditions and reaction time of Figure 4. In that case there is very little depletion of silane, so the SiH_4 and H_2 concentrations are approximately equal to their initial values, steady-state nucleation is occurring, and the rate-limiting kinetic bottleneck can be identified as the growth from seven- to eight-silicon containing clusters. The nucleation rate is then simply the rate of formation of the eight-silicon-containing clusters, which are formed by insertion of seven-silicon-containing silylenes into SiH_4. The nucleation rate is approximately equal to the total rate of the three reactions

$$Si_7H_{12}B + SiH_4 \rightarrow Si_8H_{16} \quad (6)$$

$$Si_7H_{10}B + SiH_4 \rightarrow Si_8H_{14} \quad (7)$$

$$Si_7H_8B + SiH_4 \rightarrow Si_8H_{12} \quad (8)$$

The Si_7H_x species are in partial equilibrium with the smaller clusters, so their concentrations can be calculated from eq 5. Rate constants for reactions 6−8 can be obtained directly from the rate estimation rules of Table 3. The nucleation rate calculated by this method is 5.6×10^{-15} mol/(cm^3 s), in essentially perfect agreement with the results of the detailed simulation. At given temperature and pressure, this rate depends only on the silane and hydrogen concentrations. For conditions with non-steady-state nucleation or substantial silane depletion, such a simple calculation of the nucleation rate is not possible. However, other simplified approaches can still be developed for particular nucleation regimes where one or a few kinetic bottlenecks in the overall nucleation process can be identified or where many of the clusters are in partial equilibrium with each other.

V. Summary and Conclusions

A detailed kinetic mechanism for formation of silicon hydride clusters that lead to particle nucleation during silane pyrolysis has been developed. This mechanism is capable of predicting nucleation rates at given reaction conditions and can be used in identifying the reaction pathways that lead to particle formation. A group additivity scheme, fit to results of extensive ab initio calculations, was used to estimate the cluster thermochemistry. The most stable clusters of each stoichiometry and reactivity type were identified and included in a kinetic model of clustering. Reactivity rules for the clusters were developed based on the reaction thermochemistry and the known chemical kinetics of analogous reactions of smaller silicon hydrides. Application of these rules gave estimated rate parameters for the clustering reaction mechanism. The mechanism was used to simulate time-dependent cluster formation during silane pyrolysis in the absence of any surface reactions. The results of these simulations were used to identify regimes of steady-state nucleation and non-steady-state nucleation and to delineate the most important reaction paths in each case. Under some conditions, a nucleation-rate-limiting kinetic bottleneck was observed for the formation of an eight-silicon-containing cluster. The most abundant clusters were predicted to have compact polycyclic structures composed of five- and six-membered rings.

Acknowledgment. This work was supported by Advanced Silicon Materials, Inc., Moses Lake, WA. We are grateful to the Minnesota Supercomputer Institute for generous allotments of supercomputer resources and to Gernot Katzer, Alexander Sax, and colleagues at the University of Graz for providing us with detailed results of their ab initio calculations and for helpful conversations and suggestions.

References and Notes

(1) Coltrin, M. E.; Kee, R. J.; Miller, J. A. *J. Electrochem. Soc.* **1984**, *131*, 425−434.

(2) Coltrin, M. E.; Kee, R. J.; Miller, J. A. *J. Electrochem. Soc.* **1986**, *133*, 1206−1213.

(3) Coltrin, M. E.; Kee, R. J.; Evans, G. H. *J. Electrochem. Soc.* **1989**, *136*, 819−829.

(4) Ho, P.; Breiland, W. G. *J. Appl. Phys.* **1988**, *63*, 5184−5186.
(5) Ho, P.; Coltrin, M. E.; Breiland, W. G. *J. Phys. Chem.* **1994**, *98*, 10138−10147.
(6) Breiland, W. G.; Coltrin, M. E.; Ho, P. *J. Appl. Phys.* **1986**, *59*, 3267−3273.
(7) Breiland, W. G.; Coltrin, M. E. *J. Electrochem. Soc.* **1990**, *137*, 2313−2319.
(8) Moffat, H. K.; Jensen, K. F.; Carr, R. W. *J. Phys. Chem.* **1992**, *96*, 7695−7703.
(9) Moffat, H. K.; Jensen, K. F.; Carr, R. W. *J. Phys. Chem.* **1992**, *96*, 7683−7695.
(10) Ring, M. A.; O'Neal, H. E. *J. Phys. Chem.* **1992**, *96*, 10848−10855.
(11) White, R. T.; Espino-Rios, R. L.; Rogers, D. S.; Ring, M. A.; O'Neal, H. E. *Int. J. Chem. Kinet.* **1985**, *17*, 1029−1065.
(12) Becerra, R.; Walsh, R. *J. Phys. Chem.* **1992**, *96*, 10856−10862.
(13) Becerra, R.; Walsh, R. In *Research in Chemical Kinetics*; Compton, R. G., Hancock, G., Eds.; Elsevier Science: New York, 1995; Vol. 3, pp 263−325.
(14) Becerra, R.; Frey, H. M.; Mason, B. P.; Walsh, R.; Gordon, M. S. *J. Chem. Soc., Faraday Trans.* **1995**, *91*, 2723−2732.
(15) Dzarnoski, J.; Rickborn, S. F.; O'Neal, H. E.; Ring, M. A. *Organometallics* **1982**, *1*, 1217−1220.
(16) Gordon, M. S.; Gano, D. R. *J. Am. Chem. Soc.* **1984**, *106*, 5421−5425.
(17) Gordon, M. S.; Truong, T. N.; Bonderson, E. K. *J. Am. Chem. Soc.* **1986**, *108*, 1421−1427.
(18) Gordon, M. S.; Gano, D. R.; Binkley, J. S.; Frisch, M. J. *J. Am. Chem. Soc.* **1986**, *108*, 2191−2195.
(19) Gordon, M. S.; Francisco, J. S.; Schlegel, H. B. In *Advances in Silicon Chemistry*; JAI Press: London, 1993; Vol. 2, pp 137−185.
(20) Jasinski, J. M.; Becerra, R.; Walsh, R. *Chem. Rev.* **1995**, *95*, 1203−1228.
(21) Swihart, M. T.; Carr, R. W. *J. Phys. Chem. A* **1998**, *102*, 785−792.
(22) Martin, J. G.; O'Neal, H. E.; Ring, M. A. *Int. J. Chem. Kinet.* **1990**, *22*, 613−632.
(23) Mick, H. J.; Smirnov, V. N.; Roth, P. *Ber. Bunsen-Ges. Phys. Chem.* **1993**, *97*, 793−798.
(24) Mick, H.-J.; Roth, P.; Smirnov, V. N.; Zaslonko, I. S. *Kinet. Catal.* **1994**, *35*, 439−451.
(25) Mick, H.-J.; Markus, M. W.; Roth, P.; Smirnov, V. N. *Ber. Bunsen-Ges. Phys. Chem.* **1995**, *99*, 880−890.
(26) Moffat, H. K.; Jensen, K. F.; Carr, R. W. *J. Phys. Chem.* **1991**, *95*, 145−154.
(27) Yuuki, A.; Matsui, Y.; Tachibana, K. *Jpn. J. Appl. Phys.* **1987**, *26*, 747−754.
(28) Guinta, C. J.; McCurdy, R. J.; Chapple-Sokol, J. D.; Gordon, R. G. *J. Appl. Phys.* **1990**, *67*, 1062−1075.
(29) Frenklach, M.; Ting, L.; Wang, H.; Rabinowitz, M. J. *Israel J. Chem.* **1996**, *36*, 293−303.
(30) Kruis, F. E.; Schoonman, J.; Scarlett, B. *J. Aerosol Sci.* **1994**, *25*, 1291−1304.
(31) Flint, J. H.; Haggerty, J. S. *Aerosol Sci. Technol.* **1990**, *13*, 72−84.
(32) Rao, N.; Girshick, S.; Heberlein, J.; McMurry, P.; Jones, S.; Hansen, D.; Micheel, B. *Plasma Chem. Plasma Process.* **1995**, *15*, 581−606.
(33) Herrick, C. S.; Woodruff, D. W. *J. Electrochem. Soc.* **1984**, *131*, 2417.
(34) Kelkar, M.; Rao, N. P.; Girshick, S. L. In *14th International Conference on Nucleation and Atmospheric Aerosols*; Pergammon: Helsinki, Finland, 1996; pp 117−120.
(35) Veprek, S.; Schopper, K.; Ambacher, O.; Rieger, W.; Veprek-Heijman, M. G. J. *J. Electrochem. Soc.* **1993**, *140*, 1935−1942.
(36) Slootman, F.; Parent, J.-C. *J. Aerosol Sci.* **1994**, *25*, 15−21.
(37) Ziemann, P. J.; Liu, P.; Nijhawan, S.; Kittelson, D. B.; McMurry, P. H.; Campbell, S. A. In *41st annual conference of the Institute of Environmental Science*, Anaheim, CA, 1995.
(38) Nijhawan, S.; Rao, N. P.; Kittelson, D. B.; McMurry, P. H.; Campbell, S. A.; Brockmann, J. E.; Geller, A. S. In *The ICCCS 14th International Symposium on Contamination Control*; Institute of Environmental Sciences and Technology: Pheonix, AZ, 1998; pp 270−277.
(39) Onischuk, A. A.; Strunin, V. P.; Ushakova, M. A.; Paniflov, V. N. *J. Aerosol Sci.* **1997**, *28*, 207−222.
(40) Onischuk, A. A.; Strunin, V. P.; Samoilova, R. I.; Nosov, A. V.; Ushakova, M. A.; Paniflov, V. N. *J. Aerosol Sci.* **1997**, *28*, 1425−1441.
(41) Onischuk, A. A.; Strunin, V. P.; Ushakova, M. A.; Paniflov, V. N. *Int. J. Chem. Kinet.* **1998**, *30*, 99−110.
(42) Katzer, G.; Ernst, M. C.; Sax, A. F.; Kalcher, J. *J. Phys. Chem. A* **1997**, *101*, 3942−58.
(43) Katzer, G. Personal communication.
(44) Benson, S. *Thermochemical Kinetics*; Wiley: New York, 1976.
(45) McCullough, J. P.; Pennington, R. E.; Smith, J. C.; Hossenlopp, I. A.; Waddington, G. *J. Am. Chem. Soc.* **1959**, *81*, 5880−5883.
(46) Höfler, F.; Bauer, G.; Hengge, E. *Spectrochim. Acta* **1976**, *32A*, 1435−1441.
(47) Frisch, M. J.; Trucks, G. W.; Schlegel, H. B.; Gill, P. M. W.; Johnson, B. G.; Robb, M. A.; Cheeseman, J. R.; Kieth, T.; Petersson, G. A.; Montgomery, J. A.; Raghavachari, K.; Al-Laham, M. A.; Zakrzewski, V. G.; Ortiz, J. V.; Foresman, J. B.; Cioslowski, J.; Stefanov, B. B.; Nanayakkara, A.; Challacombe, M.; Peng, C. Y.; Ayala, P. Y.; Chen, W.; Wong, M. W.; Andres, J. L.; Replogle, E. S.; Gomperts, R.; Martin, R. L.; Fox, D. J.; Binkley, J. S.; Defrees, D. J.; Baker, J.; Stewart, J. P.; Head-Gordon, M.; Gonzalez, C.; Pople, J. A. Gaussian 94 (Revision D.4); Gaussian, Inc.: Pittsburgh, PA, 1995.
(48) Zhao, M.; Gimarc, B. M. *Inorg. Chem.* **1996**, *35*, 5378.
(49) Grev, R. S.; Schaefer, H. F. *J. Am. Chem. Soc.* **1987**, *109*, 6569−6577.
(50) Ochterski, J. W.; Petersson, G. A.; Montgomery, J. A. *J. Chem. Phys.* **1996**, *104*, 2598.
(51) Nagase, S.; Kobayashi, K.; Nagashima, M. *J. Chem. Soc., Chem. Commun.* **1992**, 1302−1304.
(52) Chase, M. W. J.; Davies, C. A.; Downey, J. R.; Frurip, D. J.; McDonald, R. A.; Syverud, A. N. *J. Phys. Chem. Ref. Data* **1985**, *14*, Supp. 1.
(53) Pedley, J. B.; Beard, B. S.; Kirk, A.; Seilman, S.; Heath, L. G. *Computer Analysis of ThermoCHemical data: CATCH tables;* Sussex, England, 1972.
(54) Ritter, E. R.; Bozzelli, J. W. *Int. J. Chem. Kinet.* **1991**, *23*, 767−778.
(55) Kee, R. J.; Rupley, F. M.; Meeks, E.; Miller, J. A. *Chemkin-III: A Fortran Chemical Kinetics Package for the Analysis of Gas-Phase Chemical and Plasma Kinetics*; Sandia National Laboratories Report No. SAND96-8216; Sandia National Laboratories: Albuquerque, NM, 1996.
(56) Reynolds, W. C. *The Element Potential Method for Chemical Analysis: Implementation in the Interactive Program STANJAN*; Stanford University: Palo Alto, CA, 1986.
(57) Raghavachari, K.; Rohlfing, C. M. *J. Chem. Phys.* **1988**, *89*, 2219−2234.
(58) Ho, P.; Coltrin, M. E.; Breiland, W. G. *J. Phys. Chem.* **1994**, *98*, 10138−10147.
(59) Swihart, M. T.; Carr, R. W. *J. Phys. Chem. A* **1997**, *101*, 7434−7445.
(60) Susnow, R. G.; Dean, A. M.; Green, W. H.; Peczak, P.; Broadbelt, L. J. *J. Phys. Chem. A* **1997**, *101*, 3731−3740.
(61) Lutz, A. E.; Kee, R. J.; Miller, J. A. *SENKIN: A fortran program for predicting homogeneous gas-phase chemical kinetics with sensitivity analysis*; Sandia National Laboratories report no. SAND87-8248 Revised; Sandia National Laboratories: Albuquerque, NM, 1997.